Frictionally Modified Continental Shelf Waves and the Subinertial Response to Wind and Deep-Ocean Forcing

SCOTT B. POWER, JASON H. MIDDLETON AND R. H. J. GRIMSHAW

School of Mathematics, The University of New South Wales, Kensington, N.S.W., Australia

(Manuscript received 21 October 1988, in final form 14 April 1989)

ABSTRACT

Analytic solutions are obtained for the barotropic shelf circulation caused by wind and deep-ocean forcing at subinertial frequencies. An inclined beach model of the continental shelf is used and only situations in which bottom friction is important are considered. Three different alongshore forces are considered: pressure gradients and currents (maintained by the deep ocean) at the shelf break and wind stress over the shelf. In each case the model is formulated as a boundary value problem in which the boundary conditions are determined by the forcing mechanism. In general, a damped resonant response occurs when the forcing function has the same longshore velocity as an unforced continental shelf wave and is most significant for the first mode. In the case of forcing by an alongshore pressure gradient at the edge of the shelf, this leads to the amplification of the pressure signal towards the coast. The modal frequencies and structures are determined for various frictional values. When friction is small the results are consistent with those of Brink and Allen in that phase speeds remain unchanged and cross-shelf phase differences are introduced. At larger frictional values, however, phase speeds are reduced, and the modal structures and cross-shelf phase differences are further altered.

1. Introduction

Two types of theory have been developed by earlier workers to explain the effects of bottom friction on coastal circulation processes. One type has bottom friction dominating to the extent that time dependence is unimportant, while the second has emphasized a time-dependent (wavelike) formulation which includes bottom friction as a perturbation only.

The frictionally dominated, steady-state theories of circulation on inclined shelves due to wind stress (Csanady 1978) and oceanic alongshore pressure gradients (APGs) (Middleton 1987) are strictly valid only when the time scales of variability are long compared to the frictional spindown time (Csanady 1978; Wright 1986). The main purpose of this paper is to relax this constraint to allow for subinertial frequency variability and also to determine the response on the shelf to alongshore oceanic currents in addition to the forcing mechanisms considered above. An extensive examination of the roles played by the important parameters in the problem (bottom friction, forcing frequency and the shelf gradient) is then made.

The study of the frictional modification of barotropic continental shelf waves (CSWs) began when Gill and Schumann (1974) suggested that an allowance be made for frictional effects by including a dissipative term in the equation which governs the amplitudes of the inviscid modes in the forced response. Later, Brink and Allen (1978, 1983) confirmed the validity of this in their study in which the frictional modification was treated as a small perturbation to the inviscid equations. Their solutions showed cross-shelf phase differences in the frictionally modified CSWs, with the flow nearshore leading the flow offshore. To the lowest order, phase speeds were unaffected by friction. In the present study, the restriction to subinertial frequencies and an idealized depth profile allows the effects of both time dependence and friction to be determined analytically without restriction of the magnitude of friction. In order to better understand the results obtained, the properties of the free waves are determined and compared to the results for small friction described above.

In the case of wind-forcing, two types of shelf-break boundary conditions are considered. The reasons for this are as follows. It is usual in the study of wind-forced CSWs to solve the equations over the shelf, slope and deep ocean, apply asymptotic boundary conditions and to match the solutions using continuity of both across-shelf mass flux and pressure. In this investigation however, our primary interest lies in the response on the shelf, and to obtain a good approximation to this response in as simple a manner as possible. We circumvent the more complicated, general approach by applying conditions at the shelf break which approximate the more complete solutions under fairly typical conditions. The first type of condition imposed is that the surface displacement, ζ, is zero at the shelf break.

Corresponding author address: Scott Power, School of Mathematics, The University of New South Wales, P.O. Box 1, Kensington, New South Wales, 2033 Australia.

The solutions obtained in this manner will approximate the more general solutions provided that the transition from the shelf to the deep ocean is rapid. If this is not the case an alternative condition is required. Gill and Schumann (1974), for example, argue that the alongshore velocity, set to zero at the shelf break is appropriate for matching the oceanic and shelf flows at the outer edge of the continental margin when there are no depth discontinuities and the alongshore scale of variations greatly exceeds the shelf width. In the second case, the response to oceanic APGs is determined by matching the solution over the shelf to an alongshore sea-level slope at the shelf break. In the final case, when forcing is due to an alongshore oceanic current, it is assumed that the depth is continuous and an alongshore velocity is imposed at the shelf break. It is further supposed that a geostrophic balance exists there. This leads to a condition on ζ_x, the cross-shelf gradient of the surface displacement.

The problem is formulated in the following section and the corresponding general solution is determined in the next. The boundary conditions are then applied in section 4. The salient features of the free modes are determined and presented in section 5. The forced solutions are then reexamined in the same section. Finally, the key results are summarized and discussed in the last section.

2. Formulation

In formulating the problem, a right-handed coordinate system has been chosen such that the positive x-direction points seaward from the coast, and the y-axis lies along the straight coastline at $x = 0$ as in Fig. 1. The depth, $h(x)$, is given by

$$h = sx \tag{2.1}$$

where s is a constant that is sufficiently small that vertical motions need not be considered.

Following Wright (1986) we begin with the linearized, depth-averaged, shallow water equations for flow in a homogeneous, incompressible, barotropic and hydrostatic fluid forced by an alongshore wind stress τ. These equations are

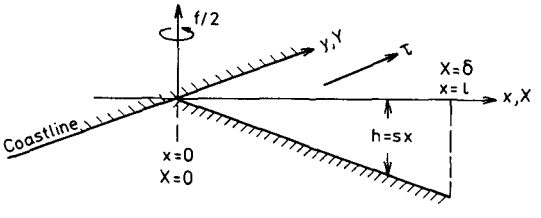

FIG. 1. Schematic diagram of the continental shelf of width l and nondimensional width δ. The cross-shelf variables are x (dimensional) and X (nondimensional). Oceanic forcing is applied at $x = l$ and wind forcing applies over the whole shelf.

$$u_t - fv = -g\zeta_x - ru/h \tag{2.2}$$

$$v_t + fu = -g\zeta_y - rv/h + \tau/\rho h \tag{2.3}$$

$$(hu)_x + (hv)_y = -\zeta_t \tag{2.4}$$

where u and v are the horizontal, depth-averaged velocity components in the x, y directions respectively; t is time; ζ is the surface displacement; g is the acceleration due to gravity; f is the Coriolis parameter (assumed constant); ρ the density and subscripts denote partial differentiation.

Bottom friction has been assumed to be proportional to the depth-averaged velocity with a constant friction coefficient r i.e.,

$$\tau_b/\rho = -r\mathbf{u}. \tag{2.5}$$

Such a parameterization scheme can be justified for subinertial motions in the presence of energetic tidal motions. The limitations and implications of this scheme have been fully discussed by Grant and Madsen (1979).

Consider motions for which

$$[u, v, \zeta] = \mathcal{R}\{[U(x), V(x), \zeta_0\eta(x)] \exp[i(ky - \omega t)]\} \tag{2.6}$$

where k is the wavenumber and ω is the frequency (allowed to take either sign) of both the forcing and the response. It can be shown that for such motions the terms u_t and $-ru/h$ in (2.2) can be neglected, provided that $(kL)^2 \ll 1$, $(\omega/f)^2 \ll 1$ and $(r/f\bar{h})^2 \ll 1$ (Wright 1986). The surface divergence can be neglected if $f^2L^2/g\bar{h} \ll 1$ (Buchwald and Adams 1968). Here L characterizes the scale over which the dependent variables change in the x-direction and $\bar{h}$ is a scale depth. Motions satisfying the above requirements can therefore be investigated with the following simplified set of equations:

$$fv = g\zeta_x \tag{2.7}$$

$$v_t + fu = -g\zeta_y + \tau/\rho h - rv/h \tag{2.8}$$

$$(hu)_x + (hv)_y = 0. \tag{2.9}$$

These three equations have been presented by earlier workers in investigations of the evolution of the coastal boundary in response to an impulsive wind stress (Birchfield and Lunde 1978; Maeland 1983).

Elimination of u and v from (2.7)–(2.9) yields the following equation for the surface displacement, ζ:

$$h_x\zeta_{xt} + h\zeta_{xxt} + fh_x\zeta_y + r\zeta_{xx} = 0. \tag{2.10}$$

Denbo and Allen (1983) have solved this equation in the case of no longshore variations in the forcing. In this paper the full equation is used to investigate three cases of coastal circulation which have different alongshore forcing mechanisms: 1) wind stress and either 2) oceanic pressure gradients or 3) oceanic currents

imposed at the shelf break. Cases 1 and 2 are time-dependent extensions of existing theories (Csanady 1978; Middleton 1987, respectively). Thompson (1987) has obtained solutions of (2.10) for case 1 for one of the two offshore boundary conditions we consider in this paper.

In each case the coastal boundary condition is that of no normal transport, i.e.,

$$hu \to 0 \quad \text{as} \quad x \to 0. \tag{2.11}$$

It follows from (2.7), (2.8) and (2.10) that

$$\frac{\tau}{\rho} - rv \to gh\left(\frac{\zeta_{xt}}{f} + \zeta_y\right) \quad \text{as} \quad x \to 0, \tag{2.12}$$

where the right-hand side is zero once it has been established that ζ and ζ_x are finite as $x \to 0$, since $h \to 0$ as $x \to 0$. Note that $\tau(x, y, t)$ is nonzero for case 1 only. If it is assumed that variations of wind stress across the shelf are not important and the wind-stress propagates alongshore then we can assume that

$$\tau(y, t) = \tau_0 \exp[i(ky - \omega t)]. \tag{2.13}$$

Solutions for realistic forcing may be found by summing contributions from appropriate frequencies, but considerable insight into the dynamics is obtained here by considering a single, arbitrary, component.

The offshore boundary conditions can be readily stipulated in terms of non-dimensional variables and their formulation is best left until after the general solution has been obtained in the following section.

3. General solution

a. Surface displacement

Substitution of (2.1) and (2.6) into (2.10) gives

$$(r - i\omega sx)\frac{d^2\eta}{dx^2} - i\omega s\frac{d\eta}{dx} + ikfs\eta = 0. \tag{3.1}$$

Transforming x to dimensionless form using $X = x/L$ where the length scale L is defined as $L = 1/k$, $k > 0$, reduces (3.1) to

$$[(\Omega X + i\epsilon)\eta']' - \eta = 0 \tag{3.2}$$

where $\Omega = \omega/f$ is a nondimensional frequency and $\epsilon = r/(fsL)$.

Setting

$$\xi(X) = 2(\Omega X + i\epsilon)^{1/2}/\Omega \tag{3.3}$$

reduces (3.2) to

$$\xi\eta'' + \eta' - \xi\eta = 0 \tag{3.4}$$

where the derivatives (primes) are now with respect to the complex variable ξ. The choice of the branch for ξ does not effect the validity of the solutions, however, the form of the solution in case 1 is simplified if the real part of ξ, $\alpha = \mathcal{R}\{\xi\} > 0$ for all X and Ω when $\delta \to \infty$. Since $\Omega X + i\epsilon$ does not vanish over the shelf at any possible modal frequency ($\epsilon \neq 0$), this choice uniquely determines ξ. Further details regarding $\xi(X)$ are left to appendix A.

Equation (3.4) is the modified Bessel equation of order zero and has linearly independent solutions I_0 and K_0, the modified Bessel functions of the first and third kinds, respectively. Thus the general solution is

$$\eta(\xi) = AI_0(\xi) + BK_0(\xi) \tag{3.5}$$

where A and B are complex constants.

b. Transport and velocity

The corresponding transports and velocities can be obtained by substituting (2.6) into (2.7) to give

$$\frac{fLX}{g\zeta_0}V(X) = X\frac{d\eta}{dX} = \tilde{V}(X) \tag{3.6}$$

say, with $\tilde{V}(X)$ being a scaled alongshore component of the volume transport. Similarly, (2.6) in (2.8) gives

$$fU(x) = \left[\left(i\omega - \frac{r}{h}\right)V(x) - igk\zeta_0\eta + \frac{\tau_0}{\rho h}\right].$$

The non-dimensional form of $hU(x)$ is given by

$$\frac{fLXU(X)}{g\zeta_0} = \frac{fLX}{g\zeta_0}\left(\frac{i\omega}{f} - \frac{r}{fsL}\frac{1}{X}\right)V - ikLX\eta + \frac{\tau_0}{\rho sg\zeta_0}$$

or

$$\tilde{U}(X) = (i\Omega - \epsilon/X)\tilde{V} - iX\eta + \hat{\tau}_0\epsilon \tag{3.7}$$

where $\tilde{U}(X) = fXU(X)/g\zeta_0 k$ has been introduced in analogy with $\tilde{V}(X)$ in (3.6) and $\hat{\tau}_0 = 1$ in case 1 (zero otherwise). Here $\zeta_0 = \tau_0/(\rho gs\epsilon)$.

Equations (3.6) and (3.7) can be used to calculate the non-dimensional transport, once $\eta(X)$ has been found. In section 4, streamlines for the scaled transport $(\tilde{U}, \tilde{V})$ are presented. Reference is made to $\Psi(X)$, the scaled transport streamfunction, defined by $\Psi_Y = \tilde{U}$ and $\Psi_X = -\tilde{V}$.

The complex functions I_m, were calculated using the International Mathematical Subroutine Library (IMSL) subroutine DCBINS. The K_m were calculated from either their power series representation, recurrence relations or asymptotic forms. The properties of modified Bessel functions used in this paper can be found in Abramowitz and Stegun (1965).

4. Boundary conditions and the corresponding solutions

a. The coastal boundary conditions

Elimination of $v(0)$ from the nondimensional form of (2.12) gives

$$\frac{d\eta}{dX} = 1 \tag{4.1}$$

in case 1 if $\zeta_0 = \tau_0 fL/\rho rg$ and

$$\frac{d\eta}{dX} = 0 \tag{4.2}$$

in cases 2 and 3 provided that $r \neq 0$ ($\epsilon \neq 0$).

b. The offshore boundary conditions

Consider matching the flow on a shelf of width l, and depth h_1 at the shelf-break with an ocean of depth h_2 in which the geostrophic balance is disturbed only by an alongshore wind-stress. Matching pressure and mass flux then leads to $h_1\zeta_{xt} + r\zeta_x + f(h_1 - h_2)\zeta_y = 0$, so that $\eta_x = 0$ if $h_1 = h_2$ and $\eta \to 0$ if $h_2 - h_1 \to \infty$. Both these boundary conditions are used in the case of wind forcing. In each case the solution is constrained at $x = l$ or $X = l/L = \delta$, the nondimensional shelf width. We now consider each case in turn.

In case 1 the two types of offshore boundary conditions considered are:

$$\text{(a)} \quad \eta(\delta) = 0 \tag{4.3}$$

and $v(\delta) = 0$. i.e.,

$$\text{(b)} \quad \left.\frac{d\eta}{dX}\right|_{X=\delta} = 0. \tag{4.4}$$

In case 2, $\zeta_y = P$ where $P = P_0 \exp[i(ky - \omega t)]$ is the alongshore, sea-level slope at $X = \delta$. Choosing $\zeta_0 = P_0/k$ gives

$$\eta(\delta) = -i. \tag{4.5}$$

If it is assumed that a geostrophic balance exists between fv and $g\zeta_x$ at the shelf-break, the condition in case 3 reduces to

$$\frac{d\eta}{dX} = 1 \tag{4.6}$$

if $\zeta_0 = fV_0L/g$. Equations (4.1), (4.2), (4.4) and (4.6) can be readily given in terms of $\eta(\xi)$ since $d\xi/dX = 2/\Omega\xi$ and so

$$\frac{d\eta}{dX} = \frac{2}{\Omega\xi}\frac{d\eta}{d\xi}.$$

c. The solutions

The resulting conditions, together with their corresponding solutions are as follows:

1) THE WIND FORCED SOLUTIONS

In case 1 $\eta_\xi(\xi(0)) = (i\epsilon)^{1/2}$. Here the same choice of branch is made as for ξ (section 3). In case 1a, $\eta(\delta) = 0$ while $\eta_\xi(\xi(\delta)) = 0$ in case 1b.

The solutions are given by

$$\mathbf{A}_{1a} = \begin{pmatrix} A \\ B \end{pmatrix}_{1a} = \frac{(i\epsilon)^{1/2}}{\Delta_{1a}} \begin{pmatrix} K_{01} \\ -I_{01} \end{pmatrix} \tag{4.7}$$

$$\mathbf{A}_{1b} = \begin{pmatrix} A \\ B \end{pmatrix}_{1b} = \frac{-(i\epsilon)^{1/2}}{\Delta_{1b}} \begin{pmatrix} K_{11} \\ I_{11} \end{pmatrix} \tag{4.8}$$

where the notation $K_{10} = K_1(\xi(0)), I_{11} = I_1(\xi(\delta))$ etc., has been introduced. Also, $\Delta_{1a} = I_{10}K_{01} + I_{01}K_{10}$ and $\Delta_{1b} = I_{11}K_{10} - I_{10}K_{11}$. The solutions in case 1a have been obtained independently by Thompson (1987).

On a semi-infinite shelf, the wind-driven response for which $\eta \to 0$ as $X \to \infty$ (or $\eta_x \to 0$), is given by

$$\eta(X) = -(i\epsilon)^{1/2}K_0(\xi)/K_{10}. \tag{4.9}$$

In Fig. 2, contours of the (a) surface displacement, $\eta(X)$ and (b) transport-streamfunction, $\Psi(X)$, are presented for case 1a where the offshore boundary condition is taken to be zero surface elevation. The contour interval is chosen to be the same for all plots, within a given figure. For example, in Fig. 2a the interval is fixed at 0.1 while in Fig. 2b it is fixed at 0.2. In these, and similar diagrams, the coastline is coincident with the y-axis at $X = 0$. We find it convenient to introduce $\sigma = \Omega/\delta_c$, $\delta_c = kL_c$ and $L_c = (r/kfs)^{1/2}$ so that $\sigma = (\omega/f)/(kL_c)$ represents a dimensionless phase speed. The length scale L_c is in fact $\sqrt{2}$ times the length scale chosen by Csanady (1978) and Middleton (1987). Three different values of σ are considered; -3.5, 0 and 3.5. The case $\sigma \approx 0$ approximates Csanady's arrested topographic wave solution in which the nearshore flow obeys a balance between windstress, bottom friction and alongshore pressure gradient, with the flow in the same direction as the wind over the majority of the coastline. Offshore, the flow is governed by Ekman dynamics and is perpendicular to the wind.

For $\sigma = 3.5$, both the transport and surface displacement are reduced in amplitude compared to their values for $\sigma \approx 0$. Significant displacements are concentrated closer to shore. Amplitudes of both ζ and Ψ are greatest for $\sigma = -3.5$ where the forcing moves in the same direction as subinertial free modes propagate (see section 5).

In order to interpret the results it is useful to define phase and response functions for the surface displacement and the alongshore component of the transport. The response functions are (unnormalized) amplitudes, while the phase functions are defined by

$$\phi_\eta(X; \sigma) = \tan^{-1}(\mathcal{I}\{\eta\}/\mathcal{R}\{\eta\})$$

$$\phi_V(X; \sigma) = \tan^{-1}(\mathcal{I}\{\tilde{V}\}/\mathcal{R}\{\tilde{V}\})$$

which represent temporal (or spatial in y) phase differences between the response and the forcing. Since both ζ and the longshore transport are porportional to $e^{-i\omega t}$, $\phi > 0$ ($\phi < 0$) indicates that the response lags the forcing when $\sigma > 0$ ($\sigma < 0$).

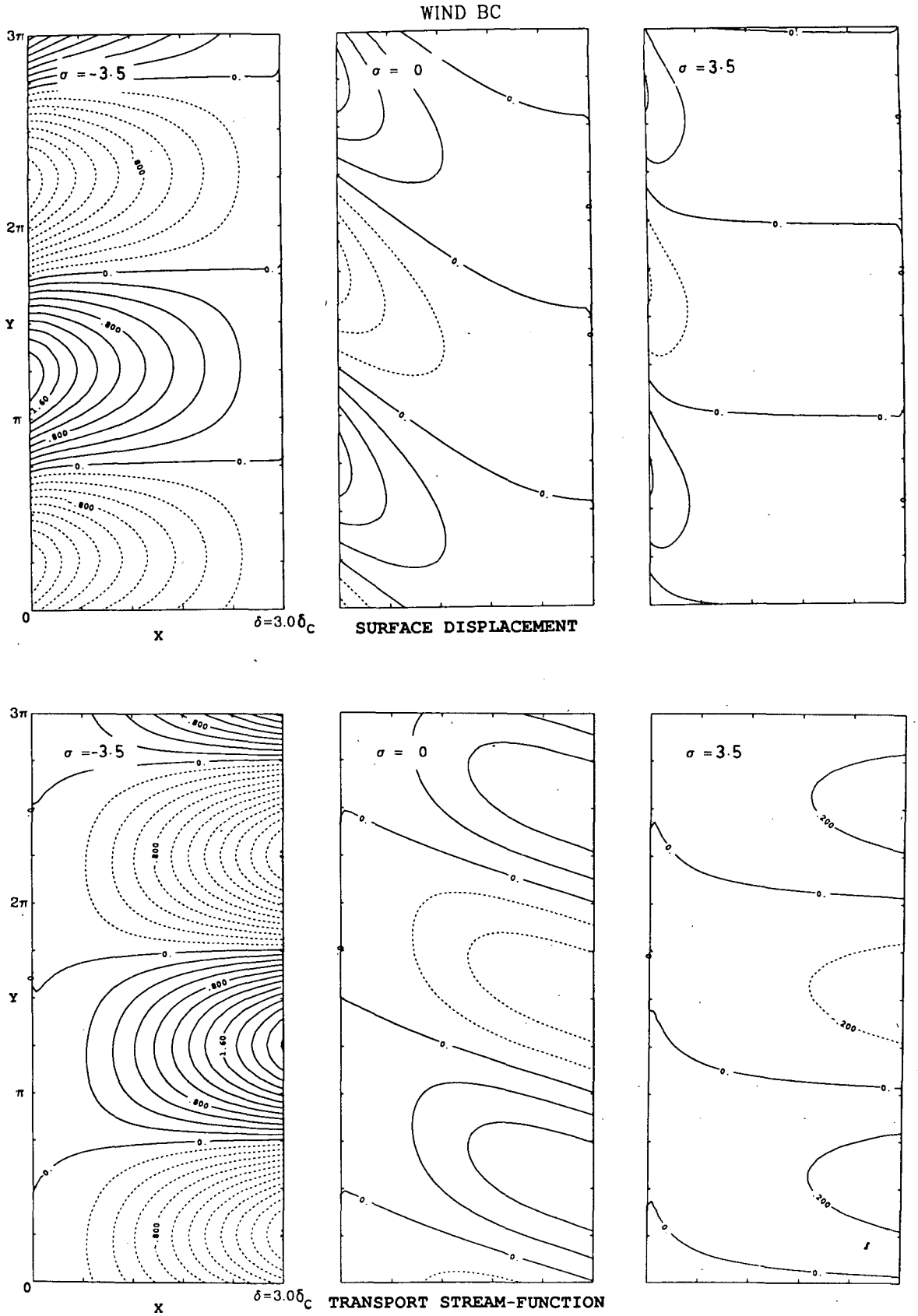

FIG. 2. Case 1a (windstress applied, $\eta = 0$ at the shelf break) (a) Surface displacement and (b) transport streamfunction contours for the dimensionless frequencies $\sigma = -3.5$, 0 and +3.5 [$\sigma = \Omega(kL_c)^{-1}$, $\Omega = \omega/f$].

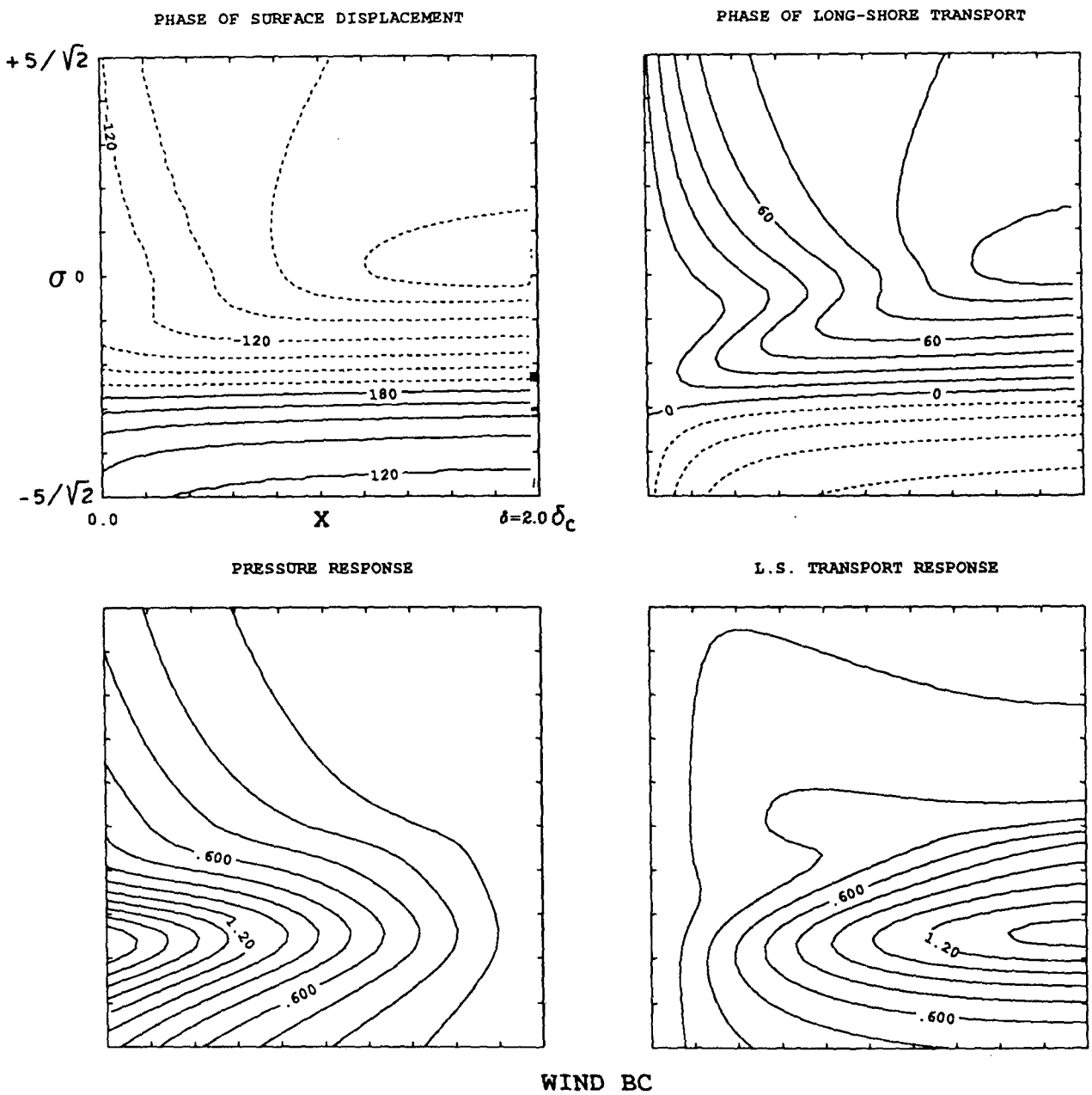

FIG. 3. Case 1a response and phase of the surface displacement and alongshore transport over the σ–X plane, with the dimensionless shelf width $\delta = 2\delta_c$.

The phase and response functions for η and $\tilde{V}$ (the alongshore component of the scaled, nondimensional transport defined in section 3) in case 1a are contoured over the range $-3.5 < \sigma < 3.5$ in Fig. 3. Both $|\eta|$ and $|\tilde{V}|$ show maxima at values of $\sigma \approx -3/\sqrt{2}$, with correspondingly rapid phase change. At $\sigma \approx -3/\sqrt{2}$, $\tilde{V}$ is in phase and η is 180° out of phase with the wind across the entire shelf. In addition, the phase changes rapidly about this point, switching sign as σ passes through $-3/\sqrt{2}$. Together, these features characterize a forced resonant response. In contrast, both phase and response functions show relatively small changes for $\sigma > 0$.

In Fig. 4, contours of the surface displacement are presented for case 1b in which the alongshore current is set to zero at $X = \delta$. When $\sigma \geq 0$ the solutions differ only in minor detail to their case 1a analogues in Fig. 2. At $\sigma = -3.5$, the transports remain similar. In con-

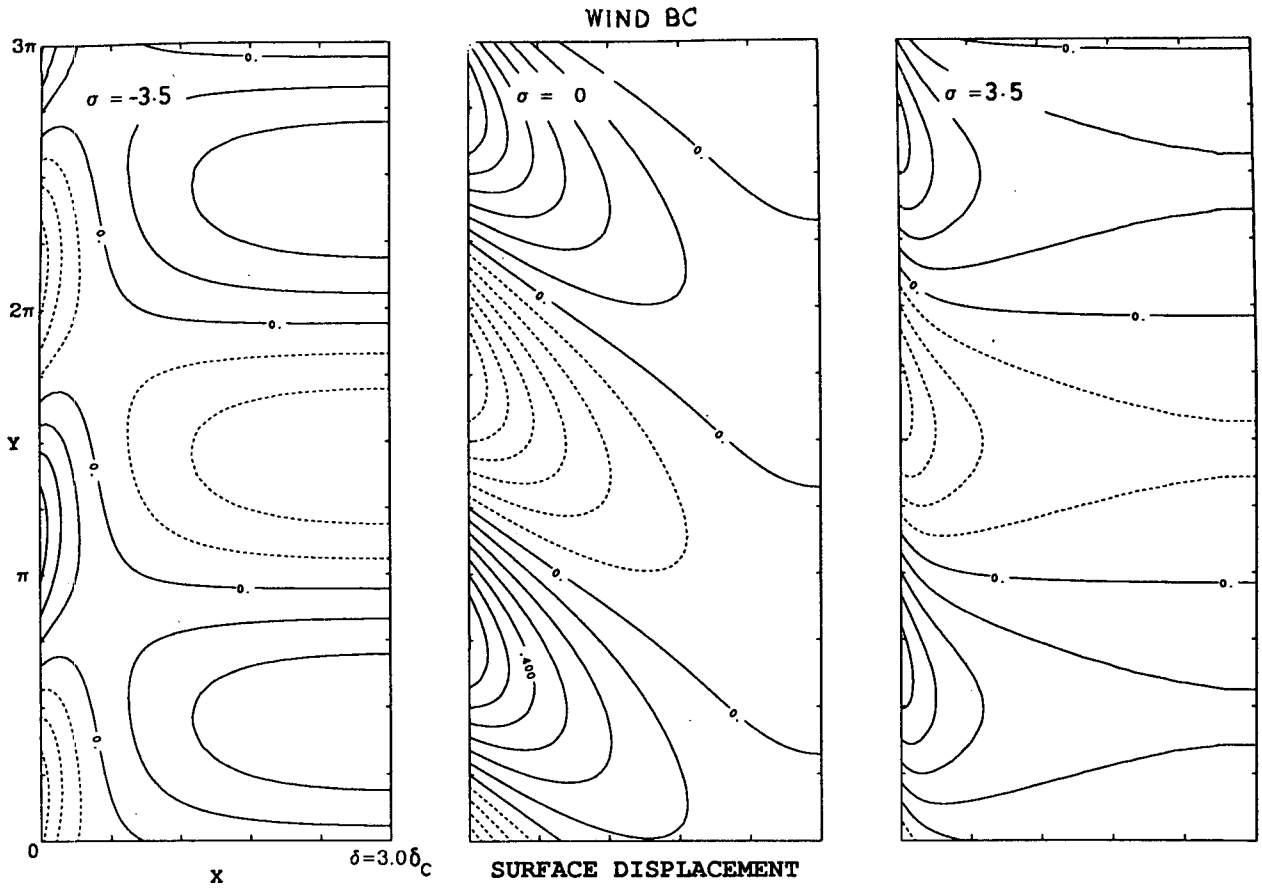

FIG. 4. Case 1b (wind stress applied, $\eta_x = 0$ at the shelf break). The surface displacement contours for $\sigma = -3.5$, 0 and +3.5.

trast, the surface displacement has a distinct double structure with maximum amplitudes at the coast, in a narrow nearshore band. Amplitudes then increase with X over most of the shelf, with secondary maxima at the shelf break. Unlike the case 1a solution, the response at $\sigma \approx 0$ is greater than at $\sigma = -3.5$.

In Fig. 5 the phase and response functions for η and $\tilde{V}$ in case 1b are contoured over the $\sigma - \delta$ plane. The surface displacement nearshore leads the offshore signal when $\sigma > 0$. When $\sigma < 0$ however, the opposite is true, with cross-shelf phase differences exceeding 90°. As σ is reduced from zero, the region of phase change is concentrated closer to shore. There is little phase change except in the range $-1/\sqrt{2} < \sigma < 0$. Again, there is a forced resonant response, but this time at $\sigma \approx -0.57$ for $\tilde{V}$. It is interesting to note that while surface displacements are largest here, over most of the shelf there is no rapid phase change passing through 0°. On the other hand ϕ_V changes rapidly near $\sigma = -0.57$. Also, when $\sigma > -0.57$ ($\sigma < -0.57$) V leads (lags) the forcing.

In Fig. 6 the phase and response functions for an infinitely wide shelf are presented. Maximum $|\eta|$ and $|\tilde{V}|$ occur when $\sigma < 0$, however no resonances are in evidence. This is discussed in more detail in section 5 and appendix B.

2) THE OCEANIC APG FORCED SOLUTIONS

In case 2, $\eta_\xi(\xi(0)) = 0$ and $\eta(\xi(\delta)) = -i$. Manipulation then gives

$$\mathbf{A}_2 = \begin{pmatrix} A \\ B \end{pmatrix}_2 = \frac{-i}{\Delta_2} \begin{pmatrix} K_{10} \\ I_{10} \end{pmatrix} \tag{4.10}$$

where $\Delta_2 = \Delta_{1a}$.

Contours of the surface displacement are presented in Fig. 7. As before, values of $\sigma = -3.5$, 0 and 3.5, with $\delta/\delta_c = 2$ are chosen. When $\sigma \approx 0$ we recapture the steady solutions obtained by Middleton (1987), which indicate a reduction in the surface displacement from the outer shelf to the coast. A similar result holds for $\sigma = 3.5$, although the maximum coastal elevation is now directly opposite that at the shelf break, and the overall transport is weaker. At $\sigma = -3.5$, however, the results are dramatically different. The surface displace-

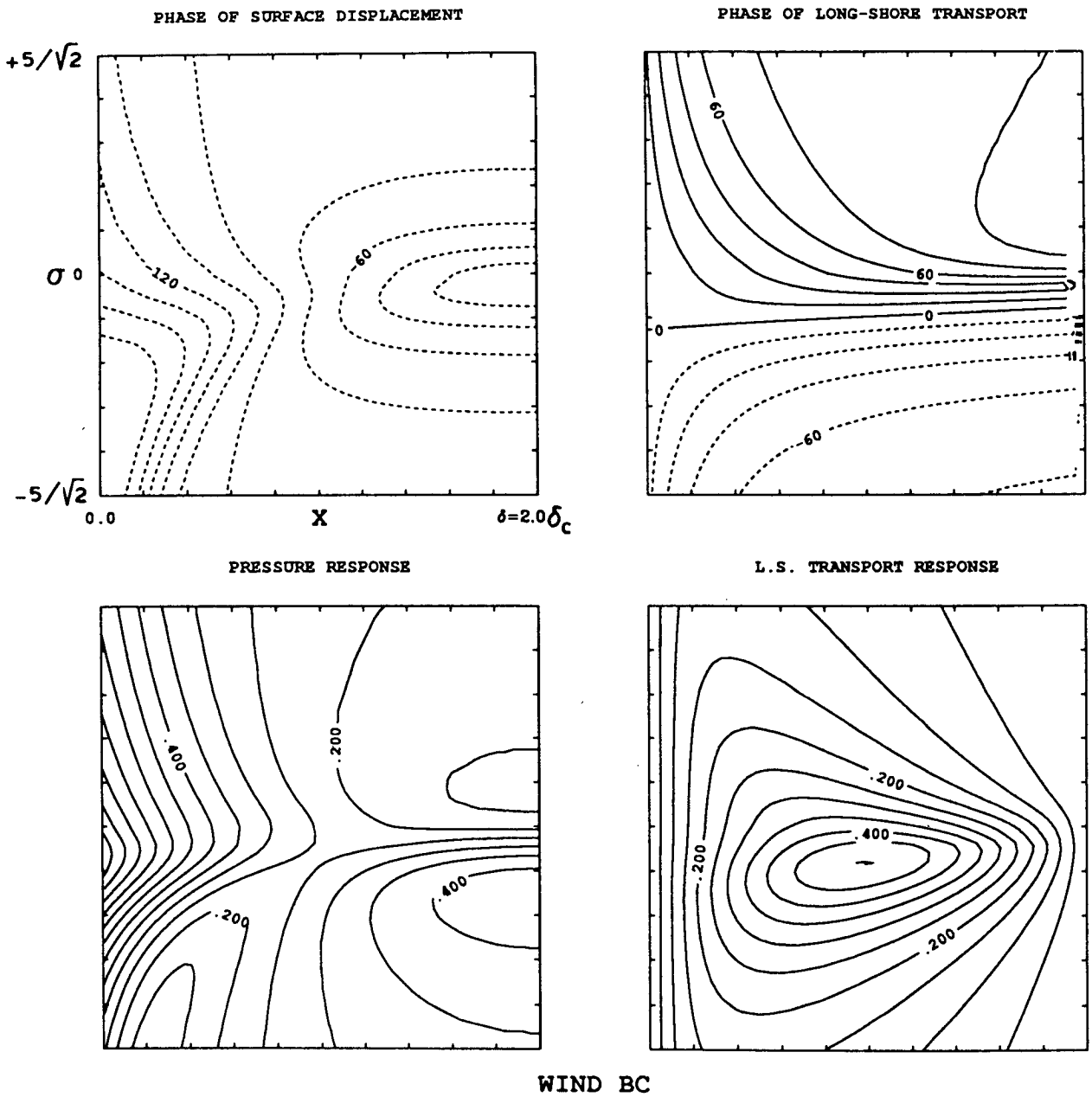

FIG. 5. Case 1b, response and phase of the surface displacement and the alongshore transport over the σ–X plane, with $\delta = 2\delta_c$.

ment near the coast is now much larger than that applied at the shelf with a correspondingly large rise in the transport. The amplification of the oceanic pressure signal across the shelf should be contrasted with the prediction of the steady model.

The cross-shelf structure of the phase and response for η and $\tilde{V}$ for a shelf of width $\delta/\delta_c = 2$ are shown in Fig. 8. As in the wind-driven case 1a the responses show clear maxima near $\sigma = -3/\sqrt{2}$: Surface displacements are larger near the coast with the response at the coast being almost four times the forcing at $X = \delta$. There is a rapid phase change (through 180°) between $\tilde{V}$ and the forcing. There is some evidence for a secondary peak in the response when σ is small and negative however it does not display any of the other characteristics of a forced resonance.

For oceanic pressure fields moving in a direction opposite to that of coastally trapped waves, the transmission of the sea-level displacement across the shelf is substantially reduced below that for $\sigma = 0$. When σ

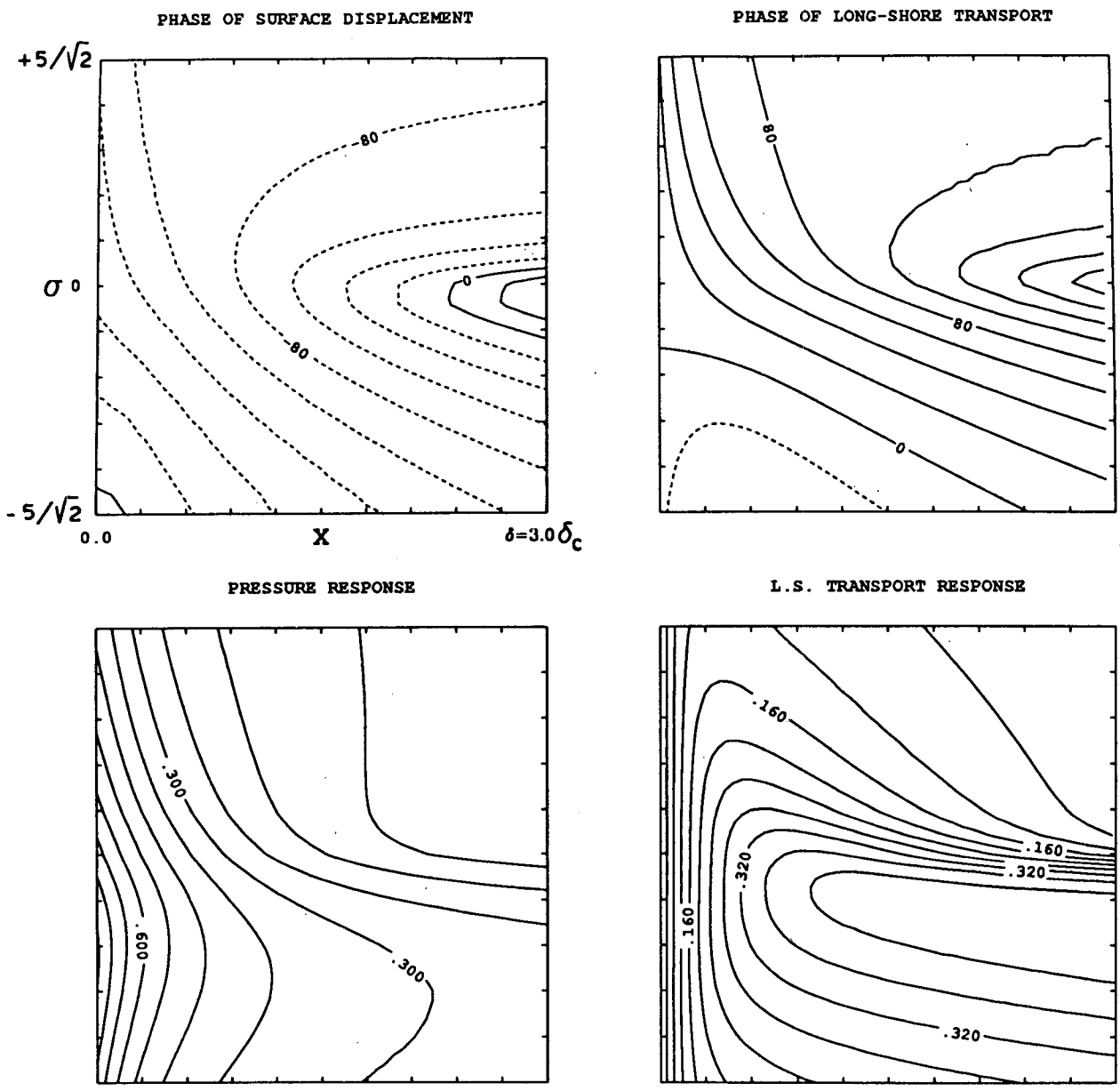

FIG. 6. Response of an infinitely wide shelf to wind forcing (Case 1 with $\delta \to \infty$). The phase and response of both the surface displacement and the alongshore transport are presented.

< 0, $\tilde{V}$ nearshore leads $\tilde{V}$ offshore. The phase difference is approximately 40° near $\sigma \approx 0$ but quickly grows to over 100° near resonance. The surface displacement nearshore leads (lags) that offshore whenever $\sigma < 0$ ($\sigma > 0$).

3) THE OCEANIC CURRENT FORCED SOLUTIONS

In a similar manner, the solution in case 3 can be shown to be given by

$$\mathbf{A}_3 = \begin{pmatrix} A \\ B \end{pmatrix}_3 = \frac{i\Omega\xi(\delta)}{2} \frac{\Delta_2}{\Delta_3} \mathbf{A}_2 \qquad (4.12)$$

where $\Delta_3 = \Delta_{1b}$. Thus $\mathbf{A}_3 = \gamma \mathbf{A}_2$ where

$$\gamma(\sigma, \epsilon) = i(\sqrt{2}\delta\sigma/\delta_c + i\epsilon)^{1/2}\Delta_2/\Delta_3. \qquad (4.13)$$

The relationship between the solutions in cases 2 and 3 can be gauged from Fig. 9 in which $|\gamma|$ and $\tan^{-1}(\mathcal{I}\{\gamma\}/\mathcal{R}\{\gamma\})$ have been contoured over the σ

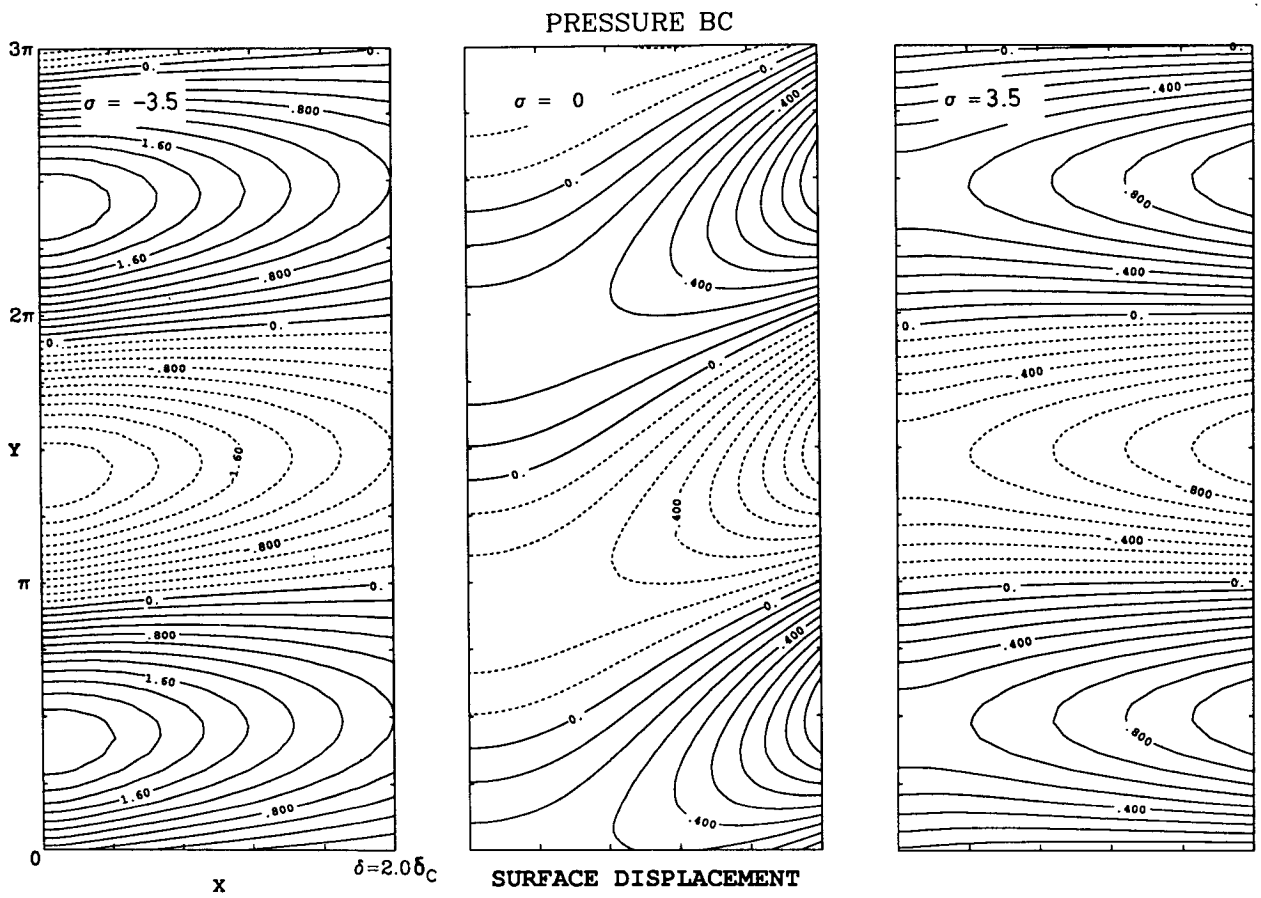

FIG. 7. Case 2. (Response to an oceanic APG). Surface displacement contours for $\sigma = -3.5$, 0 and +3.5.

$-\delta/\delta_c$ plane. The most striking feature is the weak dependence upon δ, exhibited by γ, except on very narrow shelves. In fact, for large δ/δ_c, the asymptotic behavior of $\xi(X)$ (see appendix A), $I_0(\xi)$ and $K_0(\xi)$ as $X \to \infty$ shows that $\Delta_2/\Delta_3 \to 1$ as $\delta \to \infty$, and so

$$\gamma \sim i(\sqrt{2}\delta\sigma/\delta_c + i\epsilon)^{1/2}$$

for large δ.

In order to better understand the results presented in this section, the structure and properties of the free modes are now determined.

5. Free waves and their role in the forced response

a. *The free modes*

1) MODAL FREQUENCIES

Two types of modes need to be considered:

type I having $\zeta(\delta) = 0$ (cases 1a and 2);
type II which satisfy $\zeta_x(\delta) = 0$ (cases 1b and 3).

Two important results concerning the modal frequencies can be obtained immediately.

Multiplying (3.2) by $\bar{\eta}$, the complex conjugate of η, and then integrating over the shelf leads to

$$-\Omega_n = \frac{\int_0^\delta |\eta_n|^2 dX + i\epsilon \int_0^\delta |\eta_n'|^2 dX}{\int_0^\delta X|\eta_n'|^2 dX} \tag{5.1}$$

where Ω is the nondimensional frequency of the nth mode (of either type) with cross-shelf structure $\eta_n = \eta_n(X)$. The unidirectional propagation property and the fact that only decaying modes are possible follows from the conditions that $\mathcal{R}\{\Omega_n\} < 0$ and $\mathcal{I}\{\Omega_n\} < 0$.

When the homogeneous boundary conditions satisfied by the free modes are applied, nontrivial solutions are found to be possible only if $\Delta_2 = 0$ (cases 1a and 2) or $\Delta_3 = 0$ (cases 1b and 3). These two expressions determine the dependence of the modal frequencies upon the scalded friction parameter ϵ. The $\mathcal{R}\{\Omega\}$ and $\mathcal{I}\{\Omega\}$ are measures of the phase speed and the degree of damping, respectively. The complex roots of Δ_2 and

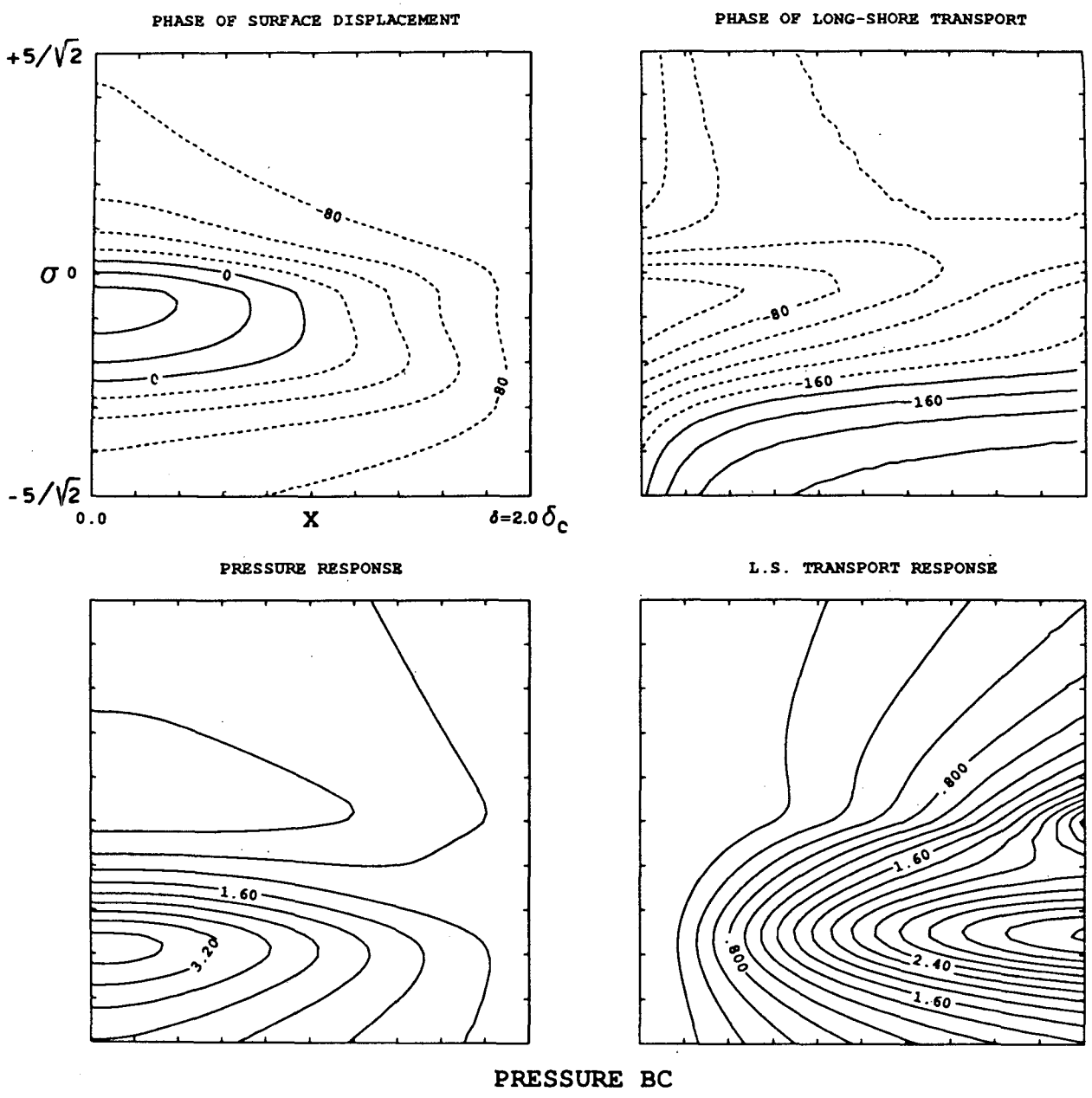

FIG. 8. Case 2. Response and phase of the surface displacement and alongshore transport over the σ–X plane, with $\delta/\delta_c = 2$.

Δ_3 have been calculated numerically and are presented in Figs. 10 and 11. Most of the important features can be obtained analytically:

Since $\delta \int_0^\delta |\eta_n'|^2 dX$ provides an upper bound on the denominator in (5.1),

$$-\frac{\int_0^\delta |\eta_n|^2 dX}{\delta \int_0^\delta |\eta_n'|^2 dX}, \quad -i\epsilon/\delta$$

provide upper bounds on the real and imaginary parts of Ω_n, respectively.

The functional $\int_0^\delta |\phi|^2 dX / \int_0^\delta X|\phi'|^2 dX$ is in fact maximized by the inviscid modal structures (Courant and Hilbert 1953), in which case it equals $|\Omega_n(\epsilon = 0)|$. Thus any modification in η will reduce this ratio, and so the phase speeds of the frictional modes are all bounded above by the phase speed of their inviscid counterparts. This result remains true for all reasonable depth profiles, by a similar argument.

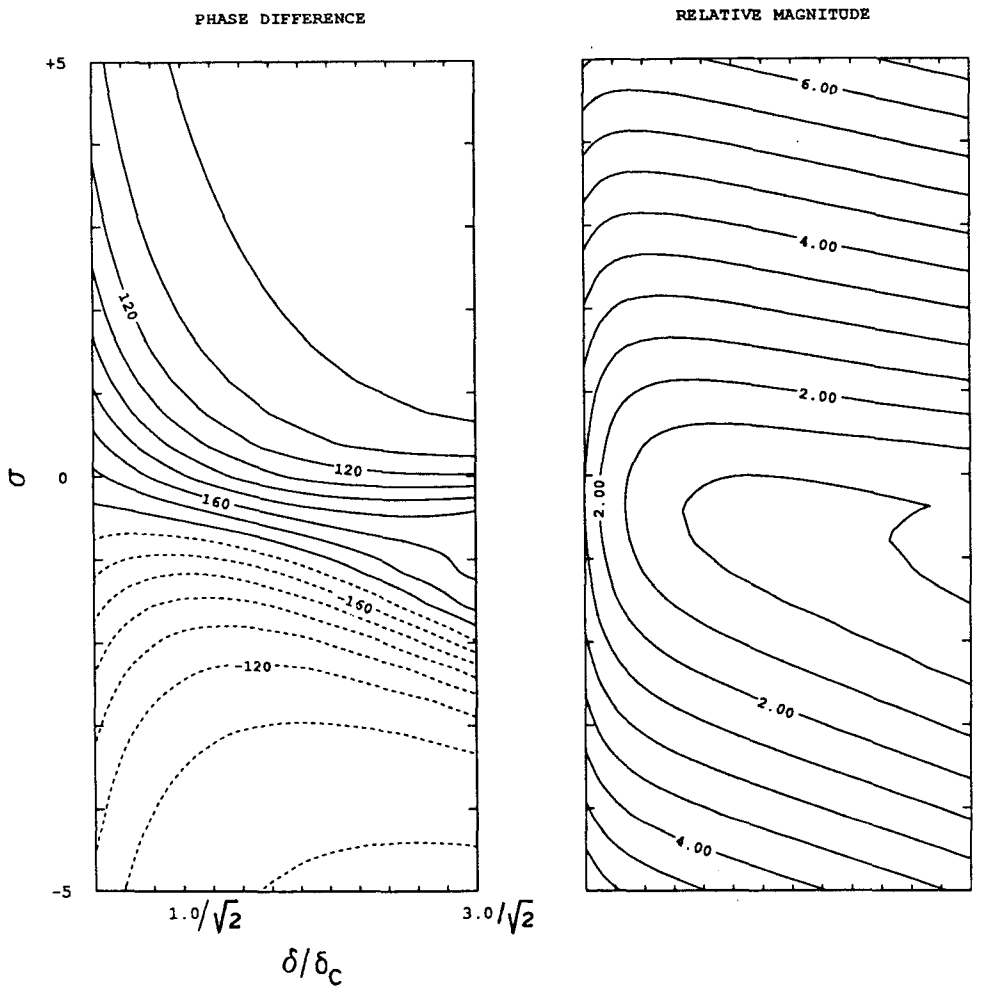

FIG. 9. Relationship between surface displacement in cases 2 and 3 as measured by $|\gamma|$ and $\tan^{-1}(\mathcal{T}\{\gamma\}/\mathcal{R}\{\gamma\})$ where $\gamma = \eta_2/\eta_3$.

In the frictionless case, $\epsilon = 0$ and $\xi(X) = 2(\Omega X)^{1/2}/\Omega$. But $K_0(X) \to \infty$ as $X \to 0$ and so the inviscid modes have $\eta = AI_0(\xi(X))$. Application of the homogeneous, offshore boundary conditions gives $I_0(2 \times (\Omega\delta)^{1/2}/\Omega) = 0$, in cases 1a and 2 and $I_1(2(\Omega\delta)^{1/2}/\Omega) = 0$, in cases 1b and 3. Thus the inviscid modes have nondimensional frequencies

$$\Omega_n = 4\delta/\mu_n^2, \quad (\mu_n^2 < 0)$$

where μ_n is the nth (nonzero) root of I_0 (type I modes) or I_1 (type II modes). In dimensional form, this yields the well-known (Pedlosky 1987) dispersion relation

$$\omega_n/f = 4kl/\mu_n^2. \tag{5.2}$$

In both Figs. 10 and 11 frequencies are scaled by their inviscid values. The figures given are the values of ϵ multiplied by 1000 for convenience. When friction is small, phase speeds remain relatively unaffected but damping is introduced in all plots. This result, found earlier by Brink and Allen (1978, 1983), holds for $r = 9.5 \times 10^{-5}$ m s^{-1} (corresponding to $\epsilon = 1.0 \times 10^{-3}$ if $f = 10^{-4}$ s^{-1}, $k = 3.14 \times 10^{-6}$ m^{-1} and $s = 3 \times 10^{-3}$) since the phase speed of the frictionally modified first type I mode is still $0.96C_1$ (where C_n is the phase speed of the nth inviscid mode) in the case where $l \approx 65$ km. On the other hand, the phase speed of the second type I mode is $0.93C_2$ when r is only 1.9×10^{-5} m s^{-1} ($\epsilon = 2.0 \times 10^{-4}$). In fact, $C = 0.5C_2$ when $r \approx 1.4 \times 10^{-5}$ m s^{-1} ($\epsilon \approx 1.5 \times 10^{-3}$).

On narrower shelves the corresponding $\Omega(\epsilon)$ for fixed k are similar to those just discussed except that damping and the reduction in phase speed are more substantial at the same ϵ. For example, if $l \approx 32$ km, the phase speed of the second type I mode is $0.5C_1$ when r is only 3.8×10^{-5} m s^{-1} ($\epsilon = 4.0 \times 10^{-4}$). Similar statements can be made for the type II modes.

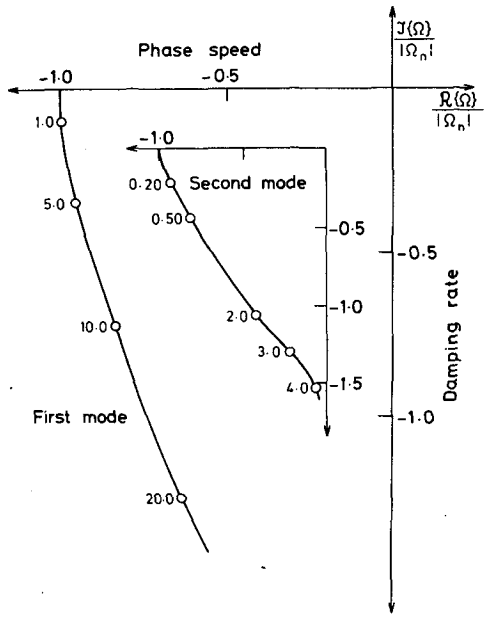

FIG. 10. Solutions of $\Delta_{1a} = \Delta_2 = 0$ which correspond to the first and second frictionally modified modes on a shelf with $l \approx 65$ km, which have $\eta(\delta) = 0$ (type I). Here, $\Omega_n = 4\sqrt{2}\delta/(\mu_n^2\delta_c)$ is the frequency of the nth inviscid mode and μ_n is the nth root of I_0. The data points represent modal frequencies at increasing values of ϵ multiplied by 1000 for convenience. $\mathcal{R}\{\Omega\}$ and $\mathcal{I}\{\Omega\}$ can be considered as the dimensionless phase speed and damping rate respectively.

2) MODAL STRUCTURE

The unnormalized modes are given by

$$\hat{\eta}_n = C_n I_0(\xi_n(X)) + K_0(\xi_n(X)) \qquad (5.3)$$

where $\xi_n(X) = 2(\Omega_n X + i\epsilon)^{1/2}/\Omega_n$ and Ω_n, the modal frequency, satisfies $\Delta(\Omega_n) = 0$ ($\Delta = \Delta_2$ for type I modes; $\Delta = \Delta_3$ for type II modes).

Type I modes have

$$C_n = -K_0(\xi_n(\delta))/I_0(\xi_n(\delta))$$

whereas the type II modes have

$$C_n = +K_1(\xi_n(\delta))/I_1(\xi_n(\delta)).$$

In Fig. 12. contours of the (a) surface displacement and (b) longshore velocity for the first mode (type I) are presented for different values of the dimensionless friction parameter ϵ. Following this, the surface displacements of mode 2 (type I) and modes 1 and 2 (type II) are presented in Fig. 13. In each case $l \approx 65$ km. In Figs. 12 and 13 the diagram at left corresponds to $\epsilon = 0$ ($r = 0$).

The cross-shelf structure of the type I(II) inviscid modes (see Pedlosky 1987, for example) are best understood in terms of the Bessel functions I_0 (I_1). The nth zero of I_0 (I_1) occupies the shelf-break position. As n increases, more and more nodes are squeezed onto the shelf. Some general comments can be made about both types of modes. When friction is included, the shelf-break position remains nodal, cross-shelf phases are introduced, and the maximum in $|V|$ jumps offshore. Maximum $|\eta|$ remain at the coast. But perhaps the single most important difference between the inviscid and frictional modes is that the latter are constrained to have $v = 0$ at the coast. As ϵ increases fruther, the cross-shelf phase difference continues to increase and the position of the maximum in $|V|$ moves further offshore. Midshelf amplitudes increase relative to their coastal values and maximum $|\eta|$ move to the midshelf. At higher values of ϵ, the second modes of both types have maximum $|\eta|$ over the midshelf, which drive strong, longshore currents locally.

b. *The resonant response*

In section 4, the phase and response functions for shelves of a particular width ($\delta/\delta_c = 2$ in fact) were presented for a range of different σ values. Maximum responses and the most rapid change in phase with σ, always occur when $\sigma < 0$. According to the inviscid theory outlined in section 5b, a series of resonant responses will occur when $(\omega_n/f)/(kl) = 4/\mu_n^2$ [from (6.9)]. When $n = 1$, this gives $(\Omega/\delta) = -0.8$ in cases 1a and 2, and -0.27 in cases 1b and 3. When friction is included, resonant responses are apparent at $\Omega/\delta \approx -0.7$ (Figs. 3 and 8) and -0.2 (Fig. 5) only. No

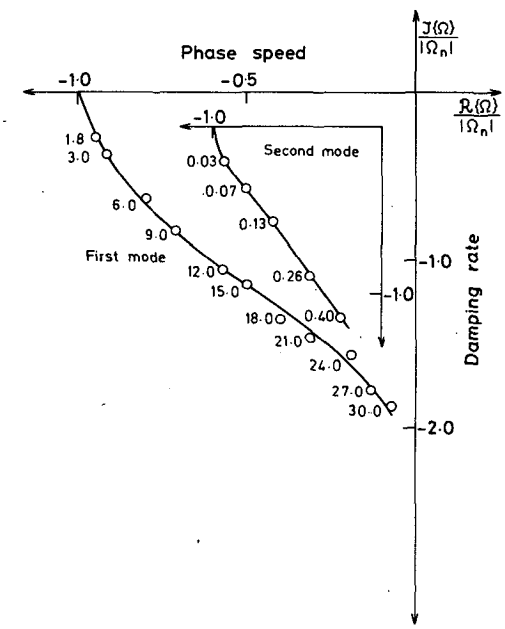

FIG. 11. Solutions of $\Delta_{1b} = \Delta_3 = 0$ which correspond to the first and second frictionally modified modes on a shelf with $l \approx 65$ km, which have $\eta_x(\delta) = 0$ (type II). $\Omega_n = 4\sqrt{2}\delta/(\mu_n^2\delta_c)$, where μ_n the nth nonzero root of I_1. The data points represent modal frequencies at increasing values of 1000ϵ.

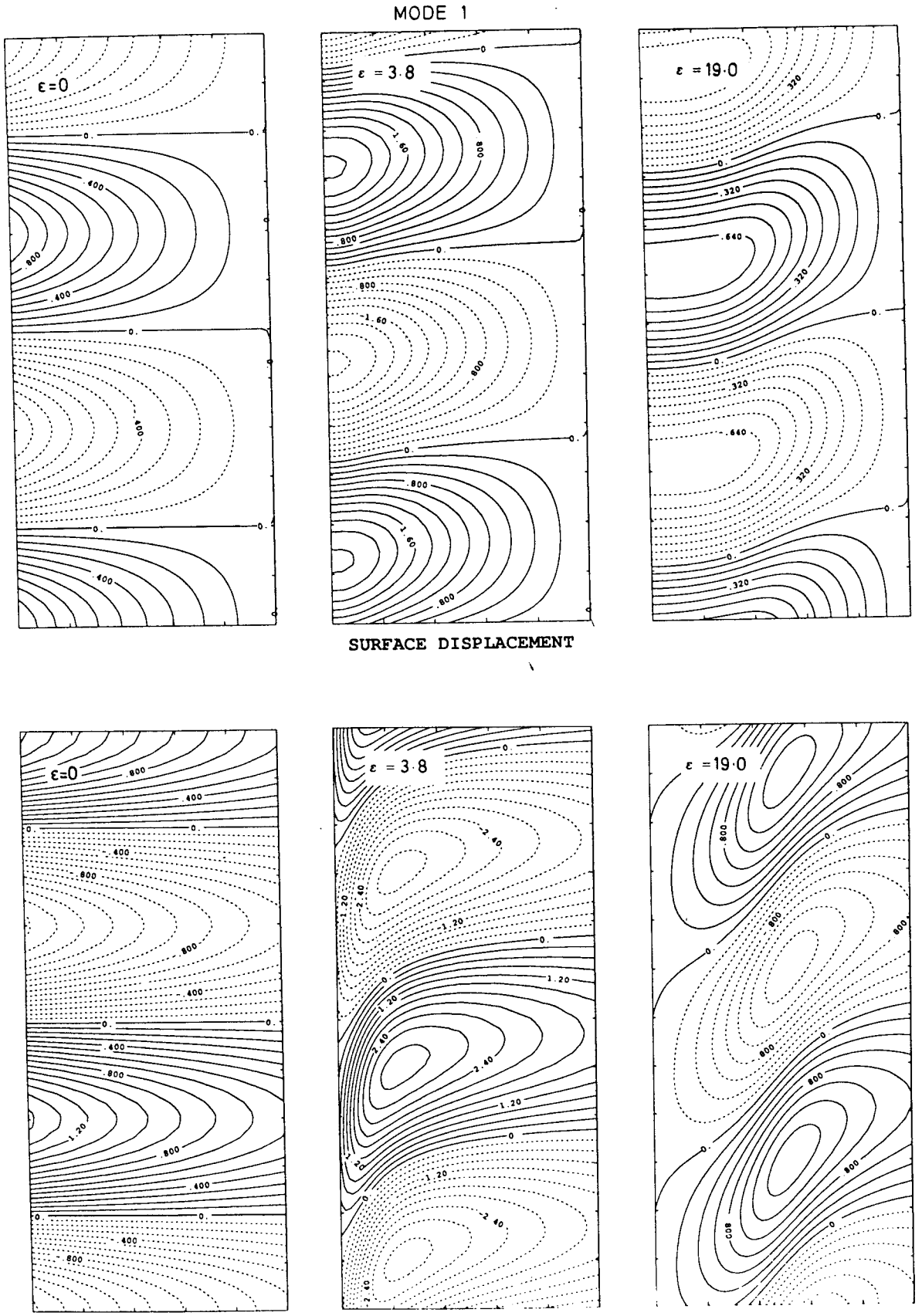

FIG. 12. (a) Surface displacement and (b) longshore, depth-averaged velocity contours for mode 1, type I [$\eta(\delta) = 0$] at increasing values of ϵ.

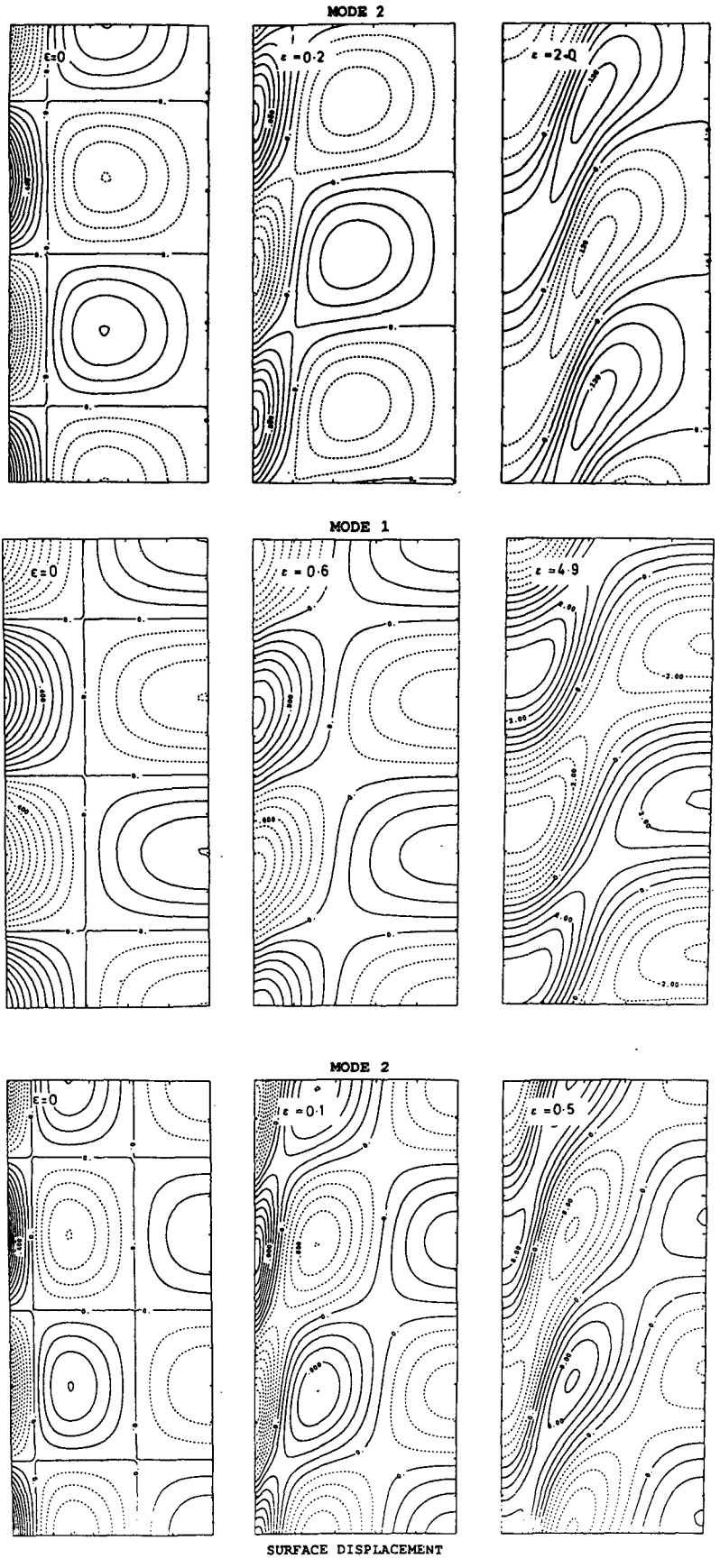

FIG. 13. Surface displacement contours for (a) mode 2, type I: $\eta(\delta) = 0$, (b) mode 1, type II $[\eta_x(\delta) = 0]$, and (c) mode II, type II $[\eta_x(\delta) = 0]$ at increasing values of ϵ.

other resonances are evident. Thus on this particular shelf at least, friction appears to have practically eliminated resonances which correspond to the modes with $n \geq 2$ for the parameter values chosen. Further, the frequency of the $n = 1$ resonance is slightly reduced from its inviscid value.

In order to determine whether or not these results have a wider applicability, response and phase functions were averaged over the shelf. Shelf-averaged results from different shelves (with nondimensional widths δ/δ_c, from 0.3 up to 3) can then be compared. For example, in Figs. 14 and 15, the shelf-averaged results for cases 1a and 2 respectively, are presented. The phase functions are now estimates of the average phase separation between the forcing and the response. A single resonance is evident when $\sigma \approx 0.2 - 1.1\ \delta/\delta_c$ (case 1a) and, $\sigma \approx -0.08 - 0.92\delta/\delta_c$ (case 2). The shelf-averaged results for cases 1b and 3 are presented in Figs. 16 and 17 respectively. Again, only a single resonance occurs when $\sigma \approx 0.08 - 1.20\delta/\delta_c$ (case 1b) and $-0.42 - 0.28\delta/\delta_c$ (case 3).

Thus friction not only reduces the rate at which the

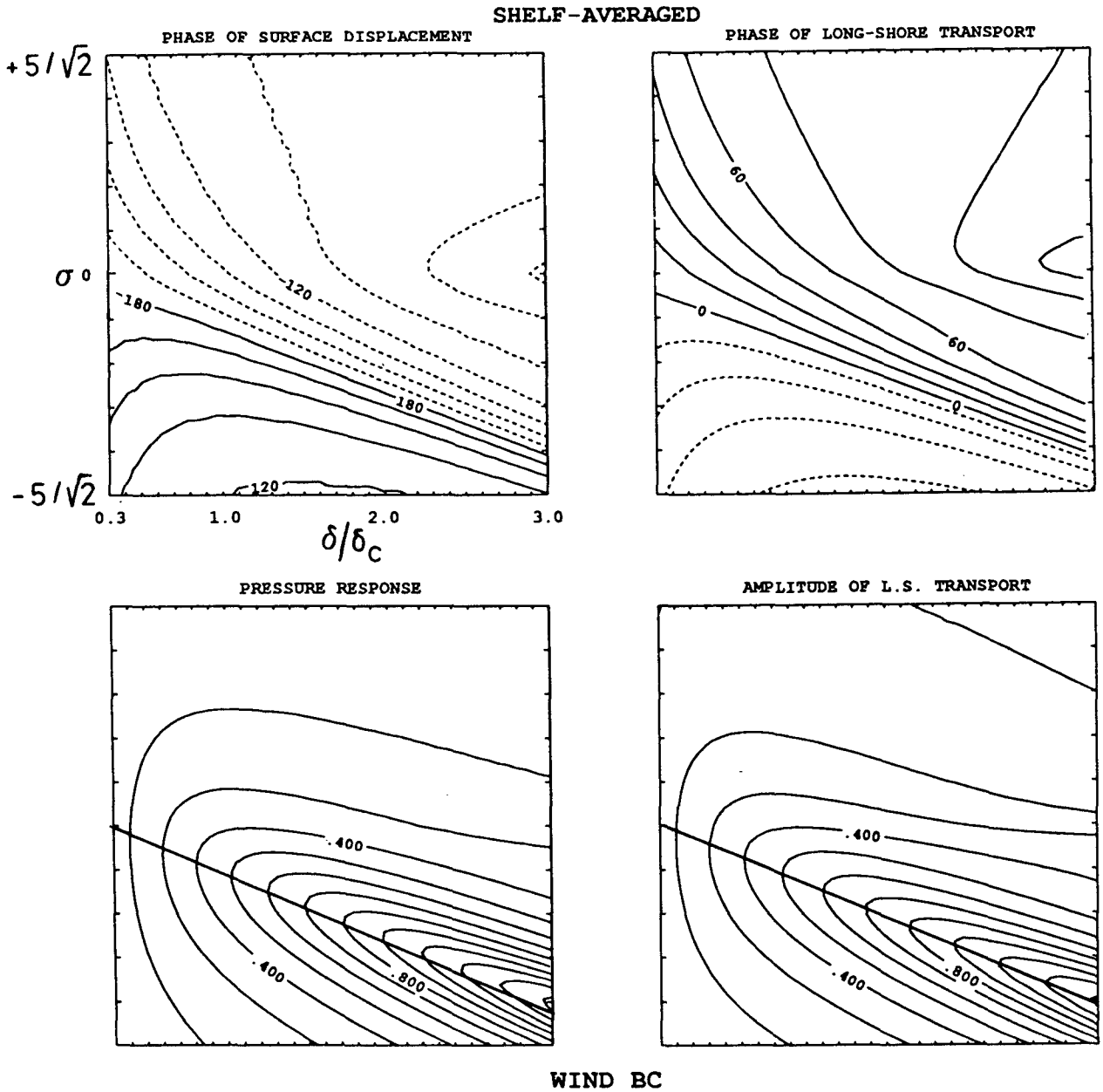

FIG. 14. Shelf-averaged phase and response functions in case 1a.

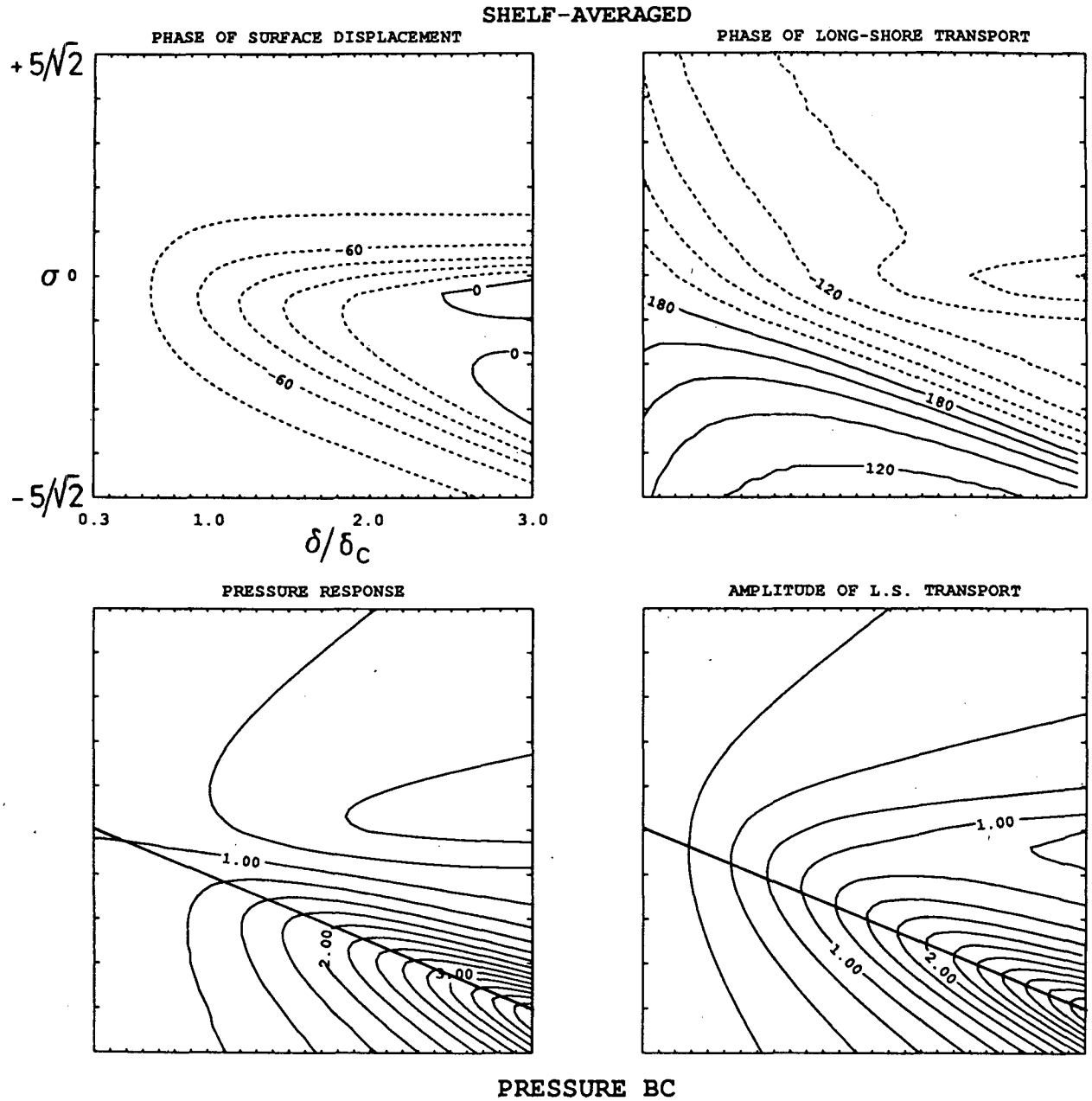

FIG. 15. Shelf-averaged phase and response functions in case 2.

resonant frequency increases as δ increases, but also shifts or detunes the resonance in frequency space, if only slightly. The line representing $\sigma = 4\sqrt{2}\delta/(\mu_1{}^2\delta_c)$, corresponding to the resonant frequency of the first inviscid mode, is shown on each of the shelf-averaged plots.

6. Discussion

The shelf circulation models of Csanady (1978) and Middleton (1987) which allow for arbitrarily large bottom friction, have been extended to allow for time-dependence at subinertial frequencies. In addition, the solution for the shelf circulation driven by a deep-ocean current has been obtained. A number of differences exist between the solutions obtained here and those given by the steady models.

When the dimensionless frequency $\Omega = \omega/f$ is positive (and the forcing function moves in the opposite direction to free wave propagation) the longshore velocity, v, and the surface displacement, ζ, are, in general, reduced compared to their steady ($\Omega = 0$) values

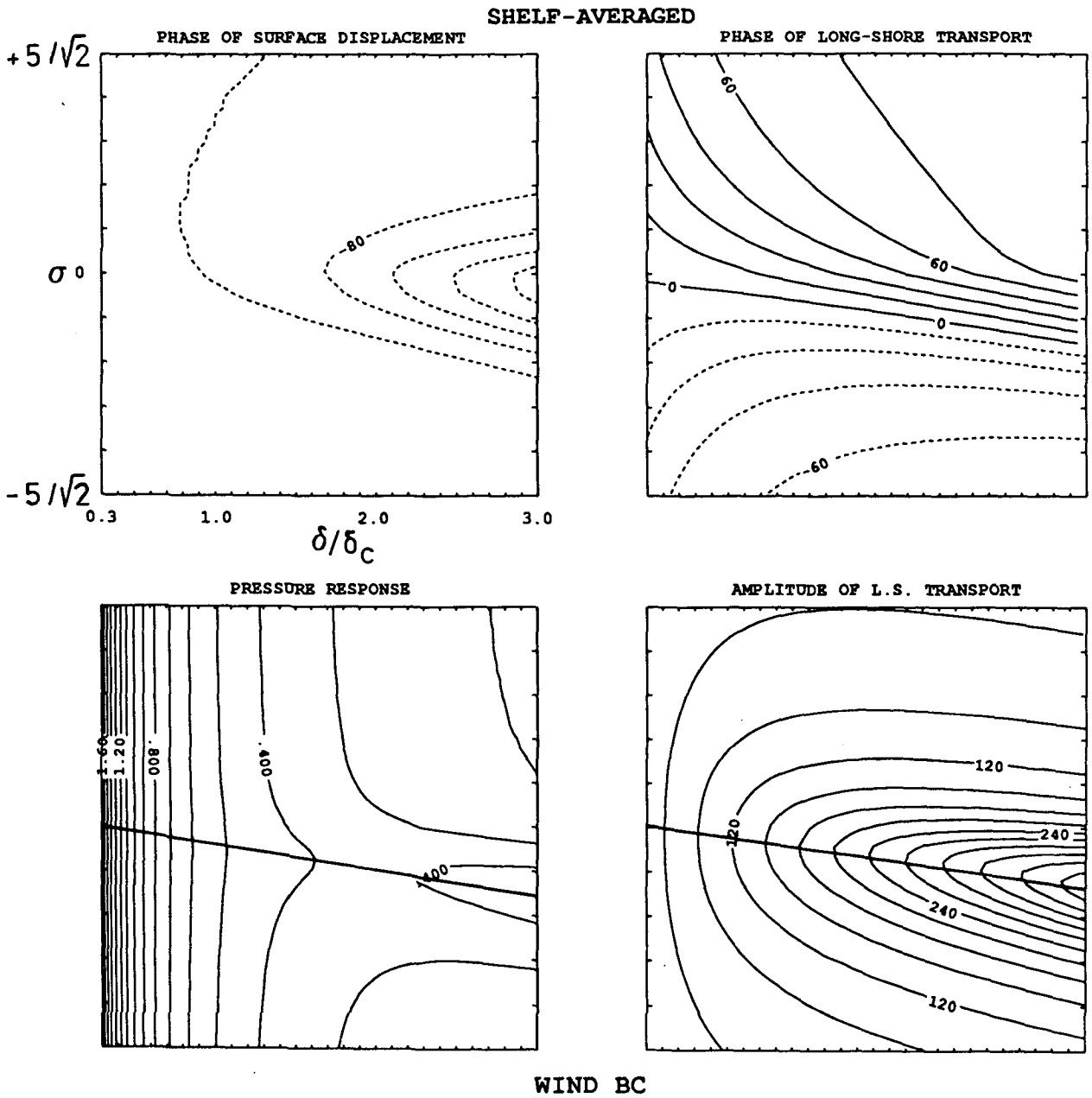

FIG. 16. Shelf-averaged phase and response functions in case 1b.

over the entire shelf. There is very little change in the phase relationship between the solution and the forcing function as Ω increases from zero, while significant surface displacements are concentrated closer to shore. In contrast, amplitudes of both ζ and v are greater when $\Omega < 0$. A single forced resonance corresponding to the first free wave is observed. The above results are common to the two types of wind-driven solutions obtained using the boundary conditions: 1a $\eta = 0$ and 1b $v = 0$ at the shelf-break. In case 1a near resonance v is in phase and η is 180° out of phase with the wind across the entire shelf and phase changes rapidly at resonance. In case 1b the single forced resonance occurs at a much lower frequency than in case 1a, when the surface displacement has a distinct double structure, with maximum amplitudes at the coast and a secondary maximum at the shelf-break. When $\Omega > 0$, the nearshore values of ζ lead those offshore. The opposite is true when $\Omega < 0$, with cross-shelf phase differences exceeding 90°. As Ω is reduced from zero, the region of significant cross-shelf phase change is concentrated closer to shore.

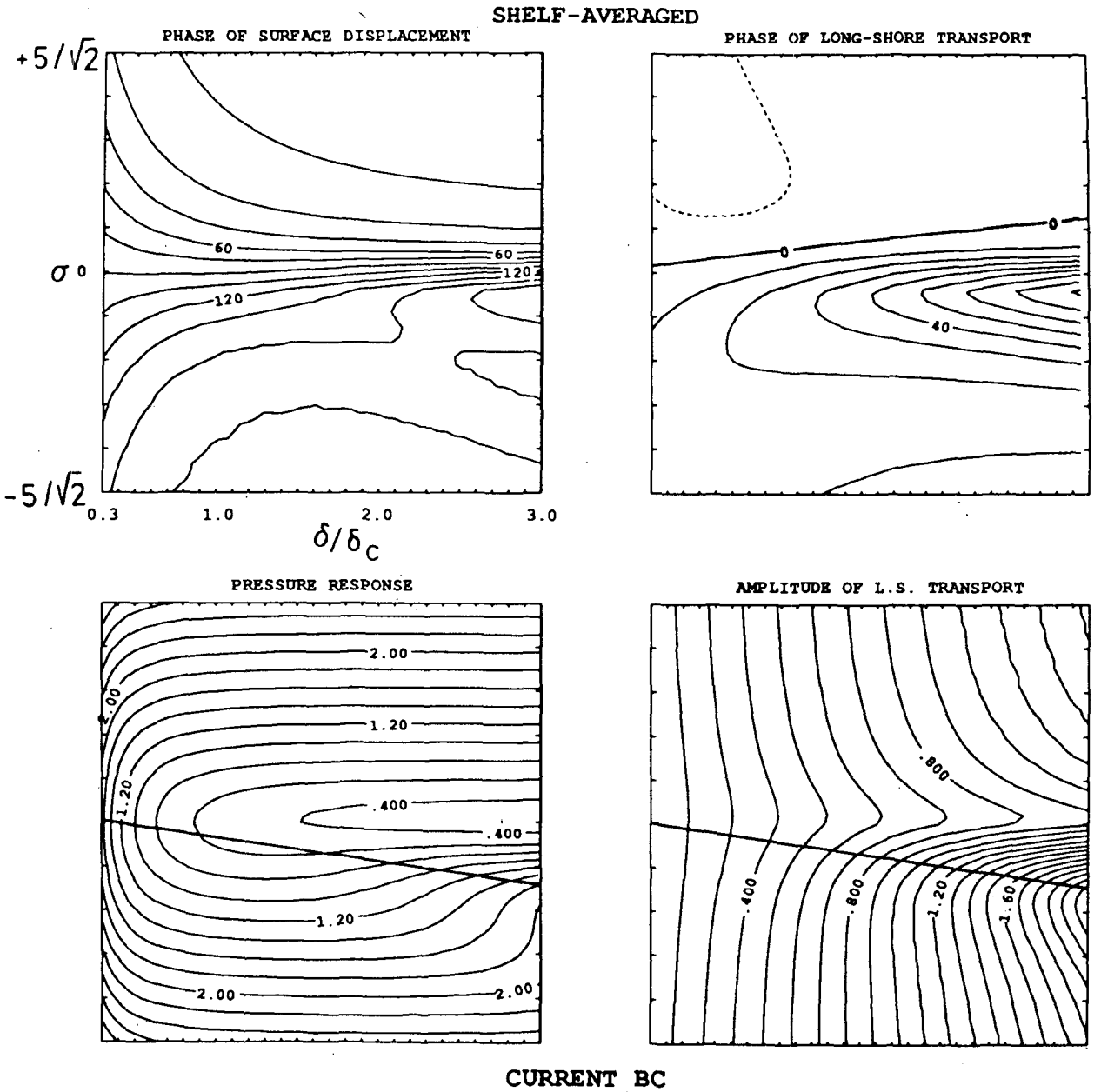

FIG. 17. Shelf-averaged phase and response functions in case 3.

In case 2, when the response is driven by an oceanic alongshore pressure gradient, the most important difference between the steady and time-dependent results occurs when $\Omega < 0$, where there is an amplification of the pressure signal across the shelf. This appears to be a new possibility, not yet described elsewhere in the literature. On the other hand, when $\Omega \geqslant 0$ the signal is diminished across the shelf. When $\Omega \gg 0$, there is very little cross-shelf phase difference in ζ, the overall transport is weaker and ζ nearshore leads ζ offshore. The opposite is true when $\Omega < 0$. The current driven solution (case 3) is simply related to the solution driven by the alongshore pressure gradient. Their surface displacements are proportional to within a known function of the two dimensionless variables σ and δ, the shelf width.

In order to better understand these results, the properties of the frictionally modified waves were determined. Two types of free waves play an important role in the forced response: type I waves having $\eta = 0$ at the shelf-break (in cases 1a and 2) and type II waves having $v = 0$ (in cases 1b and 3). The cross-shelf struc-

ture of the type I (II) inviscid modes are best understood in terms of the modified Bessel function $I_0(I_1)$. The nth zero of $I_0(I_1)$ occupies the shelf-break position. As n increases, more and more nodes are squeezed onto the shelf. When friction is included, the shelf-break position remains nodal, v is constrained to be zero at the coast with maxima in $|v|$ shifting offshore, while maximum surface displacements remain at the coast. Cross-shelf phase differences are introduced. As friction increases further, the cross-shelf phase difference increases further and the position of the maximum in $|v|$ moves further offshore. At higher values of friction, the second modes of both types have maximum $|\zeta|$ over the midshelf, which drive strong, longshore currents locally. At realistic frictional values, phase speeds, unchanged at smaller values, are reduced and damping rates increased. On narrow shelves both of these effects are more substantial, with phase speeds being reduced to only small fractions of their inviscid values.

Since resonances occur when $\Omega < 0$ it is the existence of the free modes in the time-dependent model which limits the applicability of the steady models. On the basis of inviscid shelf wave theory, one expects a succession of resonant responses as the forcing frequency passes through the modal frequencies. However, only the resonance at a frequency corresponding to the first frictionally modified mode remains clearly identifiable when damping is introduced, for the parameter values considered. This frequency is bounded above by, but closely approximates, the frequency of the first inviscid mode.

Acknowledgments. The authors thank the following people for a number of discussions on topics related to this work: Humio Mitsudera, Dave Broutman, Andrew J. Weaver, John F. Middleton, Andrew M. Moore (all at the University of New South Wales) and Ian Webster. A reviewer's comments were also helpful. This work was supported by MST Grant 85/994 and by an Australian Postgraduate Research Award.

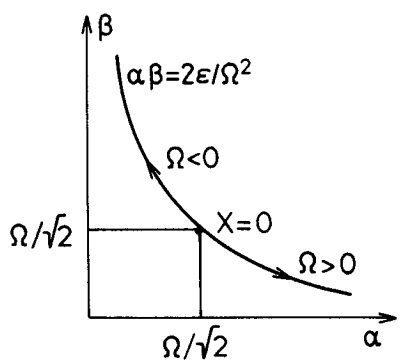

FIG. 18. The complex ξ-plane when $\Omega = \omega/f$ is real. The variable $\xi = \alpha + i\beta$, is confined to the hyperbola $\alpha\beta = 2\epsilon/\Omega^2$. The arrows indicate the behavior of ξ as X increases from zero, when $\xi = \sqrt{2}(i + 1)/\Omega$.

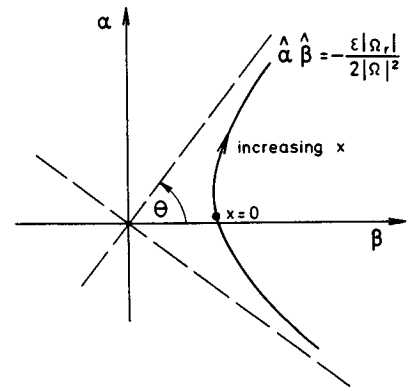

FIG. 19. The behavior of $\xi(X) = 2(\Omega X + i\epsilon)^{1/2}/\Omega = \alpha + i\beta$ when $\Omega = \Omega_r + i\Omega_i$ is complex and $\Omega_r, \Omega_i < 0$. $\xi(0)$ resides on the hyperbola $\hat{\alpha}\hat{\beta} = -\epsilon|\Omega_r|/(2|\Omega|^2)$ as shown. The angle $\theta = (\arg\Omega)/2$. As X increases from zero, ξ moves in the direction indicated. The precise position is given by (A1) and (A2).

APPENDIX A

An Analysis of the Transformation Variable $\xi(X)$

For $\xi(X) = 2(\Omega X + \epsilon i)^{1/2}/\Omega = \alpha + i\beta$ it can be shown that

$$\alpha\beta = 2[(\Omega_r^2 - \Omega_i^2)\epsilon - \Omega_i X|\Omega|^2]/|\Omega|^4 \quad \text{(A1)}$$

$$\alpha^2 - \beta^2 = 4\Omega_r(|\Omega|^2 X + 2\epsilon\Omega_i)/|\Omega|^4 \quad \text{(A2)}$$

where $\Omega = \Omega_r + i\Omega_i$. In the sections preceding section 5, however, $\Omega_i = 0$ and so ξ is confined to the hyperbola $\alpha\beta = 2\epsilon/|\Omega|^2$ and $\alpha^2 - \beta^2 \to +\infty$ as $X \to \infty$, as in Fig. 18. In section 5, $\Omega_i < 0$. In this case the behavior of $\xi(X)$ as X increases from zero is most easily determined by analyzing $\hat{\xi} = \hat{\alpha} + i\hat{\beta}$ where $\hat{\xi}^2 = \Omega\xi^2/4$, i.e.

$$\hat{\xi}^2 = \left(X - \frac{|\Omega_i|}{|\Omega|^2}\right) - i\frac{\epsilon|\Omega_r|}{|\Omega|^2} \quad \text{(A3)}$$

since the behavior of $\hat{\xi}$ with complex Ω is very similar to the behavior of ξ with real Ω: $\hat{\xi}$ is confined to the hyperbola $\hat{\alpha}\hat{\beta} = -\epsilon|\Omega_r|/(2|\Omega|^2)$ where we choose the branch with $\hat{\alpha} > 0$. The variable ξ is then obtained from (A3) which gives

$$\xi = \frac{2}{|\Omega|^{1/2}}\hat{\xi}e^{(-i/2)(\arg\Omega + 2k\pi)}, \quad k = 0, 1. \quad \text{(A4)}$$

Choosing $k = 0$, multiplication by $e^{-i/2\arg\Omega}$ represents an anticlockwise rotation of $\hat{\xi}$ by an angle between $\pi/4$ and $\pi/2$ since $\arg\Omega$ lies between $-\pi$ and $-\pi/2$ when $\epsilon \neq 0$. The resulting behavior of ξ is depicted in Fig. 19.

APPENDIX B

Free Modes Do Not Exist on an Infinitely Wide Shelf

Frictionally modified modes do not exist on infinitely wide shelves of uniform slope if $h(0) = 0$.

As $X \to \infty$, both $\mathcal{R}\{\xi\}$ and $\mathcal{I}\{\xi\} \to \infty$ and $I_0(\xi)$ becomes unbounded (Abramowitz and Stegun 1965) provided that $\epsilon \neq 0$. Therefore, $\eta_n = BK_0(\xi)$ and $\eta_n'(0) = -B \cdot K_1(\xi(0))\xi_X(0) = 0$. Thus, any nontrivial solutions must have $\xi(0) = 2(i\epsilon)^{1/2}/\Omega = \mu_n$, where μ_n is the nth root of K_1. But K_1 has no zeroes for z: $|\arg z| \leq \pi/2$ and since $\xi(0)$ lies in this part of the complex plane, no free modes exist.

REFERENCES

Abramowitz, M., and I. A. Stegun, 1965: *Handbook of Mathematical Functions,* Dover, 1046 pp.

Birchfield, G. E., and A. T. Lunde, 1978: A time-dependent model of a coastal boundary layer with friction. *J. Geophys. Res.*, **83**(C12), 6155–6162.

Brink, K. H., and J. S. Allen, 1978: On the effect of bottom friction on barotropic motion over the continental shelf. *J. Phys. Oceanogr.*, **8**, 919–922; 1983: Corrigendum, *J. Phys. Oceanogr.*, **13**, 149–150.

Buchwald, V. T., and J. K. Adams, 1968: The propagation of continental shelf waves. *Proc. Roy. Soc. London,* **A305**, 235–250.

Courant, R., and D. Hilbert, 1953: *Methods of Mathematical Physics.* Vol. 1. Interscience, 561 pp.

Csanady, G. T., 1978: The arrested topographic wave. *J. Phys. Oceanogr.*, **8**, 47–62.

Denbo, D. W., and J. S. Allen, 1983: Mean flow generation on a continental margin by periodic wind forcing. *J. Phys. Oceanogr.*, **13**, 78–92.

Gill, A. E., and E. H. Schumann, 1974: The generation of long shelf waves by the wind. *J. Phys. Oceanogr.*, **4**, 83–90.

Grant, W. D., and O. S. Madsen, 1979: Combined wave and current interaction with a rough bottom. *J. Geophys. Res.*, **84**(C4), 1797–1808.

Maeland, E., 1983: On the response of a wind-driven current over a continental shelf. *J. Geophys. Res.*, **88**(C7), 4534–4538.

Middleton, J. H., 1987: Steady coastal circulation due to oceanic alongshore pressure gradients. *J. Phys. Oceanogr.*, **17**, 604–612.

Pedlosky, J., 1987: *Geophysical Fluid Dynamics.* Springer-Verlag, 710 pp.

Thompson, K. R., 1987: Time-dependent shelf circulation and the arrested topographic wave. *J. Phys. Oceanogr.*, submitted.

Wright, D. G., 1986: On quasi-steady shelf circulation driven by alongshelf wind stress and open-ocean pressure gradients. *J. Phys. Oceanogr.*, **16**, 1712–1714.